AGU PUBLICATIONS

JGR

Journal of Geophysical Research: Space Physics

RESEARCH ARTICLE
10.1002/2014JA020273

Key Points:
- Multiple PPEF occur when the IMF Bz was stable southward
- The negative ionospheric phase oscillated in the American sector
- Inhibitation of EIA was caused by O/N2 changes and DDEF

Correspondence to:
J. Liu,
liujing@mail.iggcas.ac.cn

Citation:
Liu, J., L. Liu, T. Nakamura, B. Zhao, B. Ning, and A. Yoshikawa (2014), A case study of ionospheric storm effects during long-lasting southward IMF B_z-driven geomagnetic storm, *J. Geophys. Res. Space Physics*, *119*, 7716–7731, doi:10.1002/2014JA020273.

Received 8 JUN 2014
Accepted 22 AUG 2014
Accepted article online 27 AUG 2014
Published online 9 SEP 2014

A case study of ionospheric storm effects during long-lasting southward IMF B_z-driven geomagnetic storm

Jing Liu[1,2,3], Libo Liu[1,2], Takuji Nakamura[3], Biqiang Zhao[1,2], Baiqi Ning[1,2], and A. Yoshikawa[4]

[1]Key Laboratory of Earth and Planetary Physics, Institute of Geology and Geophysics, Chinese Academy of Sciences, Beijing, China, [2]Beijing National Observatory of Space Environment, Institute of Geology and Geophysics, Chinese Academy of Sciences, Beijing, China, [3]National Institute of Polar Research, Tokyo, Japan, [4]International Center for Space Weather Science and Education, Kyushu University, Fukuoka, Japan

Abstract Multiple instrumental observations including GPS total electron content (TEC), f_oF_2 and h_mF_2 from ionosondes, vertical ion drift measurements from Communication/Navigation Outage Forecasting System, magnetometer data, and far ultraviolet airglow measured by Thermosphere, Ionosphere, Mesosphere Energetics and Dynamics/Global Ultraviolet Imager (TIMED/GUVI) are used to investigate the profound ionospheric disturbances at midlatitude and low latitude during the 14–17 July 2012 geomagnetic storm event, which was featured by prolonged southward interplanetary geomagnetic field component for about 30 h below −10 nT. In the East Asian/Australian sector, latitudinal profile of TEC variations in the main phase were characterized by three bands of increments and separated by weak depressions in the equatorial ionospheric anomaly (EIA) crest regions, which were caused by the combined effects of disturbance dynamo electric fields (DDEF) and equatorward neutral winds. In the recovery phase, strong inhibition of EIA occurred and the summer crest of EIA disappeared on 16 July due to the combined effects of intrusion of neutral composition disturbance zone as shown by the TIMED/GUVI O/N_2 measurements and long-lasting daytime westward DDEF inferred from the equatorial electrojet observations. The transit time of DDEF over the dip equator from westward to eastward is around 2200 LT. In the American longitude, the salient ionospheric disturbances in the summer hemisphere were characterized by daytime periodical intrusion of negative phase for three consecutive days in the recovery phase, preceded by storm-enhanced density plume in the initial phase. In addition, multiple short-lived prompt penetration electric fields appeared during stable southward interplanetary magnetic field (IMF) B_z in the recovery phase and were responsible for enhanced the EIA and equatorial ionospheric uplift around sunset.

1. Introduction

Several review articles have summarized the patterns and physical mechanisms of the ionospheric storms [e.g., *Prölss*, 1995; *Buonsanto*, 1999; *Richmond and Lu*, 2000; *Danilov*, 2001; *Mendillo*, 2006; *Danilov*, 2013], involving electrodynamics, neutral dynamics, and chemical reactions. It is generally accepted that negative ionospheric storms are caused by changes in neutral composition due to the heating of the thermosphere during geomagnetic storms. Ionospheric *F* region electron content production is mainly produced by the photoionization of atomic oxygen, and the recombination is determined by the density of molecular gases N_2 and O_2. Consequently, the electron density is proportional to O/N_2 when the transport process plays a secondary importance. There is a classical picture of the evolvement of neutral composition disturbance (decreased O/N_2) zone during geomagnetic storms as presented by *Burns et al.* [1989] and *Prölss* [1995]. Vertical advection at high latitudes causes the upwelling of molecular-rich air leading to a decrease in O/N_2 in the ionospheric F_2 region, and then the composition disturbance zone will be adverted horizontally toward lower latitudes in the midnight/early morning sector driven by equatorward winds due to high-latitude heating and ion drag force. At the same time, the composition disturbance zone corotates with the Earth into the dayside and recovers gradually in this process. The movement of composition disturbance zone is controlled by background circulation and storm time-generated equatorward neutral wind fields [*Fuller-Rowell et al.*, 1994]. During daytime the storm-induced equatorward winds and the background day-to-night winds are in the opposition direction but in the same direction at night. Therefore, the two atmospheric circulations cancel each other on the dayside and augment on the nightside. Thus, the composition-disturbed area is more readily to

propagate to the middle latitudes at nighttime than at daytime. However, composition bulge is difficult to propagate to the low latitudes and resultant enhancement in O/N_2 at low latitudes during low-to-moderate geomagnetic disturbances [e.g., *Liu et al*., 2012a].

Complicated patterns of ionospheric configurations may appear at midlatitude and low latitude due to the combined effects of the prompt penetration electric fields (PPEF), DDEF, enrollment of modified neutral composition, and neutral winds. Generally, PPEF are thought as the penetration of solar wind motional electric fields into equatorial ionosphere with an efficiency of about 6.6%–9.6% [*Kelley et al*., 2003; *Huang et al*., 2007] before the shielding effects of inner magnetosphere builds up [*Wolf et al*., 2007]. It takes about 30 min to build up the shielding layer but occasionally sustains as long as a few hours [e.g., *Huang et al*., 2005a, 2005b]. *Nishida* [1968] was the first to link geomagnetic DP2 fluctuations with the variations of the interplanetary magnetic field north–south component (IMF B_z) and suggested that solar wind electric fields may penetrate into the equatorial ionosphere. Since then there are lots of studies regarding to the characteristics of PPEF [e.g., *Fejer and Scherliess*, 1995; *Kikuchi et al*., 2000; *Huang et al*., 2007; *Wei et al*., 2011], their associations with the state of solar winds [e.g., *Guo et al*., 2010] and their impacts on the middle- and low-latitude ionosphere [e.g., *Mannucci et al*., 2005; *Rishbeth et al*., 2010]. DDEF are produced through the ionospheric dynamo process with time scales from a few to several hours due to the energy injection into auroral region altering the global circulation and generating disturbed electric fields [*Blanc and Richmond*, 1980; *Scherliess and Fejer*, 1997; *Fejer*, 2011]. Using multiple instrumental observations around the Jicamarca during the high-speed solar wind-driven stormy days 5–7 January 2008, *Liu et al*. [2012b] showed that daytime equatorial f_oF_2 increased with a simultaneous decrease in h_mF_2 relative to their geomagnetic quiet time values, while daytime equatorial ionization anomaly (EIA) structure was inhibited under the effects of the westward DDEF. Besides the dramatic modifications of plasmas redistribution induced by electrodynamical processes, these physical processes can also produce ionospheric scintillations due to the generation of low-latitude spread *F*. For example, a combination of PPEF and DDEF, which corresponds to postsunset and postmidnight local time zones, respectively, can cause ionospheric irregularity occurrence in extended longitude ranges of more than 180° [*Li et al*., 2010].

Apart from the influences of disturbed electrodynamics on the middle- and low-latitude ionosphere, neutral dynamics processes taking the form of large-scale thermospheric circulation or traveling atmospheric disturbances also play an important role in the plasma distribution in two ways. The storm-driven equatorward winds will push the plasmas along the magnetic field lines into higher altitudes where the plasma recombination rates are lower and hinder the diffusion of electrons along the magnetic field lines and inhibit the formation of equatorial ionization anomaly (EIA) [e.g., *Balan et al*., 2013]. *Lin et al*. [2005] has tested the relative importance of ionospheric drivers such as electric field, neutral winds, and neutral composition changes in producing low- and middle-latitude total electron content (TEC) enhancement via numerical simulation and concluded that storm time equatorward winds produce a larger TEC enhancement than that produced by the storm-generated upward $\mathbf{E}\times\mathbf{B}$ drifts during the October 2003 superstorm. *Lu et al*. [2012] made a comprehensive Thermosphere Ionosphere Mesosphere Electrodynamics General Circulation Model modeling of ionospheric variations driven by PPEF and neutral winds on 9 November 2004 and showed that neutral winds play a more important role in producing vertical ion drifts at middle latitudes than PPEF. However, relative importance of these mechanisms is variable and may change with location, season, local time, storm phase, etc. *Wang et al*. [2010] analyzed the coupled magnetosphere ionosphere thermosphere model results and showed that storm time enhancements in the daytime eastward electric field were the primary cause of the observed daytime positive storm effects at low and middle latitudes as well as the negative response around the geomagnetic equator.

This storm event has a unique characteristic in that the solar wind driver IMF B_z lasts as long as ~30 h below −10 nT. We will discuss some peculiar features of ionosphere spatial-temporal variations belonging to this storm and identify the sources of these large-scale variations. For example, we have observed the lowest value of f_oF_2 during the years 2011–2012 and long-term depression of f_oF_2 over Sanya (18.3°N, 109.6°E) in this storm event. The rest of this paper is arranged as follows. In section 2, we mainly discuss the multiple data resources, followed by the results of spatial and temporal variations of ionospheric storms utilizing ionospheric and thermospheric observations in the two chains, one in the American sector (~70°W) and the other in the Asian/Australian sector (~120°E) in section 3. In this section, we will interpret the observations according to the storm progression. The analysis of the derived results and the conclusions are given in the last two parts.

Table 1. List of the Stations Used in the Analysis

Station	Code	Geo. Lat (deg)	Geo.Lon (deg)	Dip (deg)	Geomag. Lat (deg)
			Ionosonde Data		
Mohe	MH	52.5°N	122.3°E	69.7	42.4
Beijing	BJ	40.3°N	116.2°E	58.6	30.5
Wuhan	WH	30.5°N	114.6°E	45.9	20.7
Sanya	SY	18.3°N	109.6°E	24.3	8.5
Darwin	DW	12.5°S	131.0°E	−41.2	−22.4
Townsville	TV	19.7°S	146.9°E	−48.8	−28.2
Brisbane	BR	27.1°S	153.1°E	−57.0	−34.7
Mundaring	MU	35.3°S	149.1°E	−67.0	−42.6
Hobart	HO	42.9°S	147.3°E	−72.9	−51.7
Jicamarca	JIC	12.0°S	76.8°W	−0.16	−2.2
Fortaleza	FORT	3.9°S	38.4°W	−14.8	4.3
			Magnetometer Data		
Davao	DAV	7.0°N	125.4°E	−1.2	−3.6
Manado	MND	1.4°N	124.8°E	−13.6	−9.2
Jicamarca	JIC	12.0°S	76.8°W	−0.16	−2.2
Piura	PIU	5.2°S	80.7°W	13.6	7.1
Huancayo	HUA	12.0°S	75.3°W	−1.8	−1.0
Kourou	KOU	5.2°N	52.7°W	−14.9	−5.3

2. Data Presentation

The ionospheric F_2 region critical parameters are routinely scaled at the ionosonde stations in China and Australia. The station information is shown in Table 1. The ionosonde data at Mohe, Beijing, Wuhan, and Sanya are obtained from Institute of Geology and Geophysics of the Chinese Academy of Sciences, and data at Darwin, Townsville, Brisbane, Mundaring, and Hobart are from the Ionospheric Prediction Service of Australia. Ionograms recorded at Jicamarca, which are downloaded from the Lowell Digital Ionogram Database [*Reinisch et al*., 2009], are collected to retrieve the F_2 layer critical frequency (f_oF_2) and F_2 layer peak height (h_mF_2). We have scaled the ionograms traces manually using the SAO Explorer software package based on the built-in true height inversion technique.

Three pairs of magnetometers including equatorial stations and off-equatorial stations provide a way to measure the daytime electrojet and the intensity of ionospheric F region E × B vertical drift [*Anderson et al*., 2002]. In the American longitude, difference in the magnitudes of the geomagnetic horizontal component ($dH_{JIC\text{-}PIU}$) between Jicamarca (12.0°S, 76.8°W, 0.8°N dip latitude) and Piura (5.17°S, 80.64°W, 6.8°N dip latitude) is used for current analysis. And another pair of magnetometers including equatorial station Huancayo (12.05°S, 75.3°W, 1.62°S dip latitude) and the nonequatorial station Kourou (5.2°N, 52.7°W, 14.9°S dip latitude) measured horizontal component difference ($dH_{HUA\text{-}KOU}$) are used as a supplement when $dH_{JIC\text{-}PIU}$ is missing. In the East Asian sector, magnetometers including equatorial station Davao (7.0°S, 125.4°E, 1.2°S dip latitude) and the nonequatorial station Manado (1.4°N, 124.8°E, 13.6°S dip latitude) that measured horizontal component difference ($dH_{DAV\text{-}MND}$) are used.

The Communication/Navigation Outage Forecasting System (C/NOFS) satellite was launched on 17 April 2008 into an elliptical orbit at 401–865 km altitudes with an inclination of 13°. It takes about 66 days for this spacecraft to cover all local times. There are six onboard instruments on C/NOFS including planner Langmuir probe, vector electric field instrument, neutral wind monitor, ion velocity monitor, GPS receiver for remote ionospheric sensing, and radio beacon. Ionospheric plasma drift velocities used in present analysis are measured by Ion Velocity Meter (IVM). V_z component around the magnetic equator measured by IVM instrument is used as an indicator of equatorial zonal electric field. The accuracy of this measurement depends on the percentage of O^+, and the most reliable ion drift meter measurement come in the region near perigee and on the dayside. We used 30 min average value of the vertical plasma drifts within 5° of the dip equator during the 13–17 July 2013, ignoring the altitude variation of vertical plasma drifts.

The Global Ultraviolet Imager (GUVI) is one of the instruments on board NASA TIMED satellite in order to investigate the far ultraviolet airglow of major components from the upper atmosphere. This satellite has been launched into a 630 km circular polar orbit in 2001, with an inclination of 74.1°. The satellite progresses

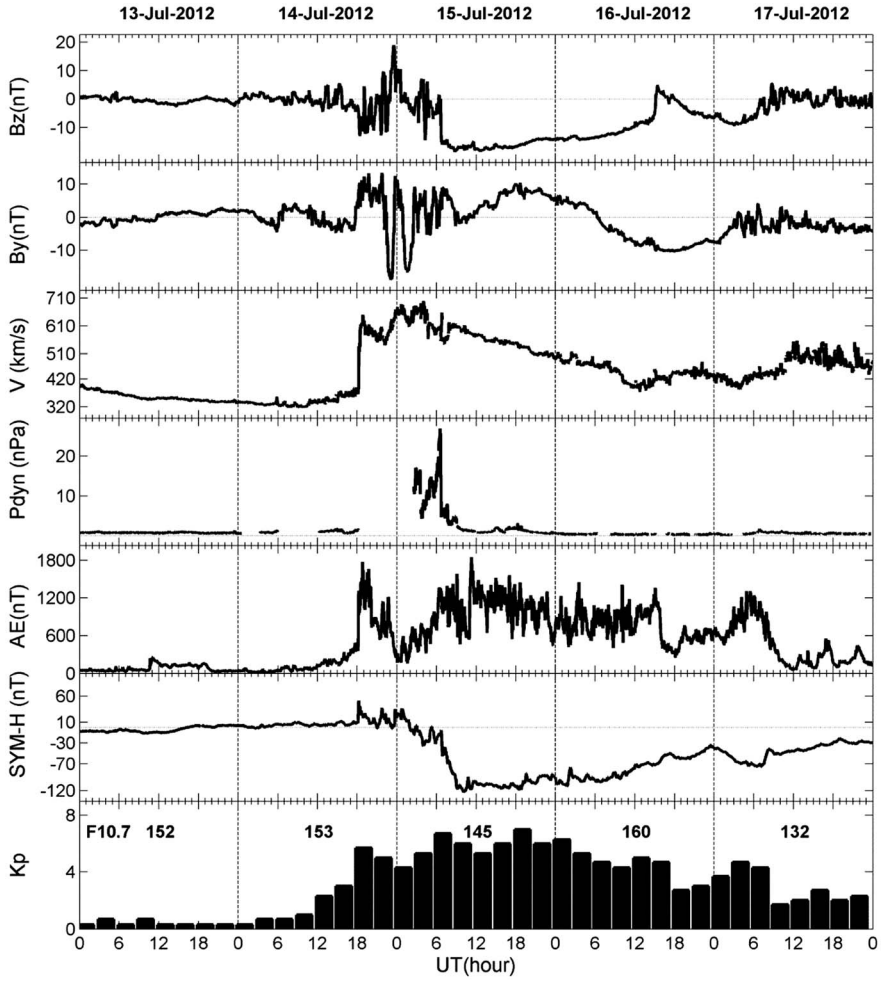

Figure 1. Interplanetary magnetic field B_z and B_y components in the GSM coordinate, solar wind velocity (V), solar wind dynamic pressure (*P*dyn), *AE* index, *SYM-H* index, and *Kp* index during 13–17 July 2012. The $F_{10.7}$ index is labeled in the lowest panel.

at a rate of 3° d^{-1} and almost samples a constant local time in a few days. The column O/N_2 ratio is reflected by OI 135.6 nm and N_2 Lyman-Bridge-Hopfield dayglow brightness ratio in the nadir direction above an altitude of about 130 km where the N_2 column density equals to 10^{17} cm^{-2} [*Christensen et al*., 2003; *Strickland et al*., 2004]. The column O/N_2 ratio is used to indicate the neutral composition changes and its impact on the electron contents.

The GPS TEC data are retrieved from the International Global Navigation Satellite System Service GPS tracking network. Slant TEC observations are used to convert to vertical TEC data of 2.5° grid via least squares fits and nearest neighbor interpolation method over the East Asian/Australian (~120°E, LT = UT + 8) and American sectors (~70° W, LT = UT − 5). The detailed procedures for GPS TEC were described by *Mao et al*. [2008]. JPL-provided TEC was described in detail elsewhere [*Liu et al*., 2010] and was also used to get the composite picture as TIMED/GUVI progression.

3. Observations and Interpretations

3.1. Solar-Terrestrial and Geomagnetic Disturbance Conditions

Figure 1 illustrates the evolutions of interplanetary magnetic field B_z and B_y components in the GSM coordinate, solar wind velocity (*V*), solar wind dynamic pressure (*P*dyn), *AE* index, *SYM-H* index, and *Kp* index during 13–17 July 2012. The solar wind data are obtained from ACE satellite measurement and shifted by

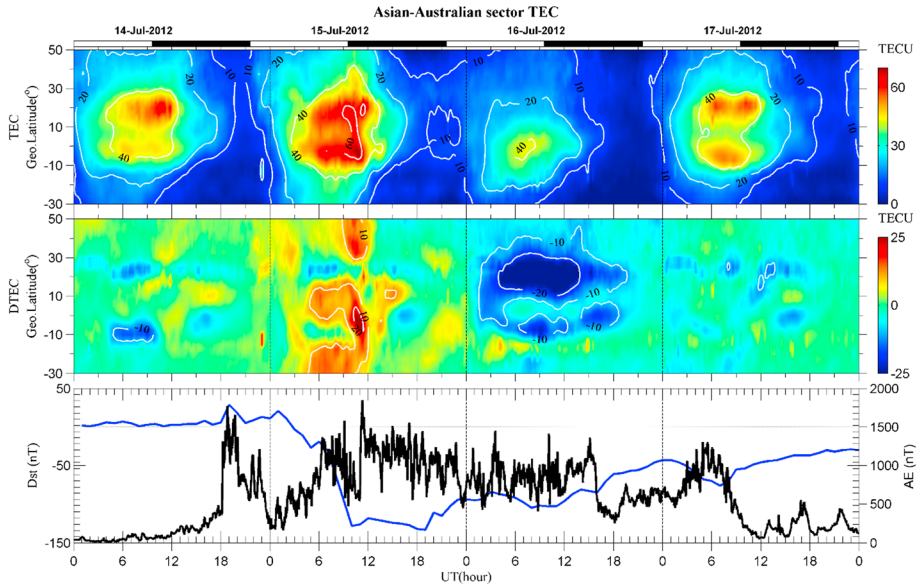

Figure 2. (top) TEC and (middle) the deviations of TEC (DTEC) with respect to the value at the same UT on 13 July derived from GPS network in the Asian/Australian sector (~120°E) on 14–17 July 2012. (bottom) The variations of *Dst* and *AE* indices.

44 min given the time lag of solar wind propagation from L1 point to the magnetosphere. The symmetric component of ring current (*SYM-H*) can be viewed as a high-resolution version of *Dst* index, *AE* index roughly represents the auroral energy inputs, and *Kp* index describes geomagnetic conditions at middle latitudes.

The IMF B_z and B_y were close to zero, the solar wind pressure and solar wind speed were small and stable, and magnetic activity was very weak on 13 July. Thus, the ionospheric parameters on 13 July were used as a quiet time reference. Shock-like changes in the solar wind parameters occurred at ~ 1726 UT on 14 July 2012. Almost simultaneously, the *AE* index experienced an abrupt increase to the maximum value ~1800 nT, and *Kp* index reached 5.7. After the SSC, the IMF B_z changed between northward and southward within the range from ~ −10 nT to 10 nT, B_y component also oscillated, and solar wind speed kept at a relative high level ~ 600 km/s. The geomagnetic storm main phase commenced at about 0640 UT on 15 July. The *SYM-H* index attained the minimum −123 nT at 1016 UT 15 July and then recovered gradually, and *AE* index got its maximum value 1851 nT. During the main and early recovery phase, the solar wind was characterized by a long-term (~32 h) and large southward IMF B_z component, gradual changing IMF B_y component from positive to negative values, and smoothly decreasing solar wind speed.

3.2. Ionospheric Response Features in the Chinese-Australian Sector

3.2.1. Multiband Increments in TEC and Quasi-Periodical Oscillations of f_oF_2/h_mF_2 in the Storm Main Phase

Figure 2 shows storm time UT geographic latitude distributions of TEC (top) and the deviations of TEC (DTEC) (middle) with respect to the reference values on 13 July derived from GPS network in longitude ~120°E and *Dst* index (bottom) on 14–17 July 2012. Geomagnetic equatorial TEC (~10°geographic latitude) enhancements of about 10 total electron content unit, 1 TECU = 10^{16} el m^{-2} (TECU), during the periods 0400–1100 UT 15 July were sandwiched by double crests depletion ~ 8 TECU. At higher latitudes above the crest regions, TEC increased with the maximum value of about 10 TECU in both hemispheres. A meridional ionosonde chain spanning from northernmost to southernmost in Chinese mainland was also used to investigate the ionospheric F_2 region response features, as shown in Figure 3. Periodical structures with periods of 2–3 h were seen both in the curves of h_mF_2 and f_oF_2 from ~1800 UT 14 July to 1200 UT 15 July. The h_mF_2 were moderately elevated in MH and BJ and showed complex variations in WH. h_mF_2 over SY decreased during 0300–0900 UT 15 July and followed by ~3 h increment as illustrated in Figure 3. Pronounced enhancements in f_oF_2 appeared at MH, BJ, WH, and SY around dusk terminator at around 1000 UT on 15 July, and this effect was more pronounced at higher latitudes and delayed at lower latitudes. Judging from the

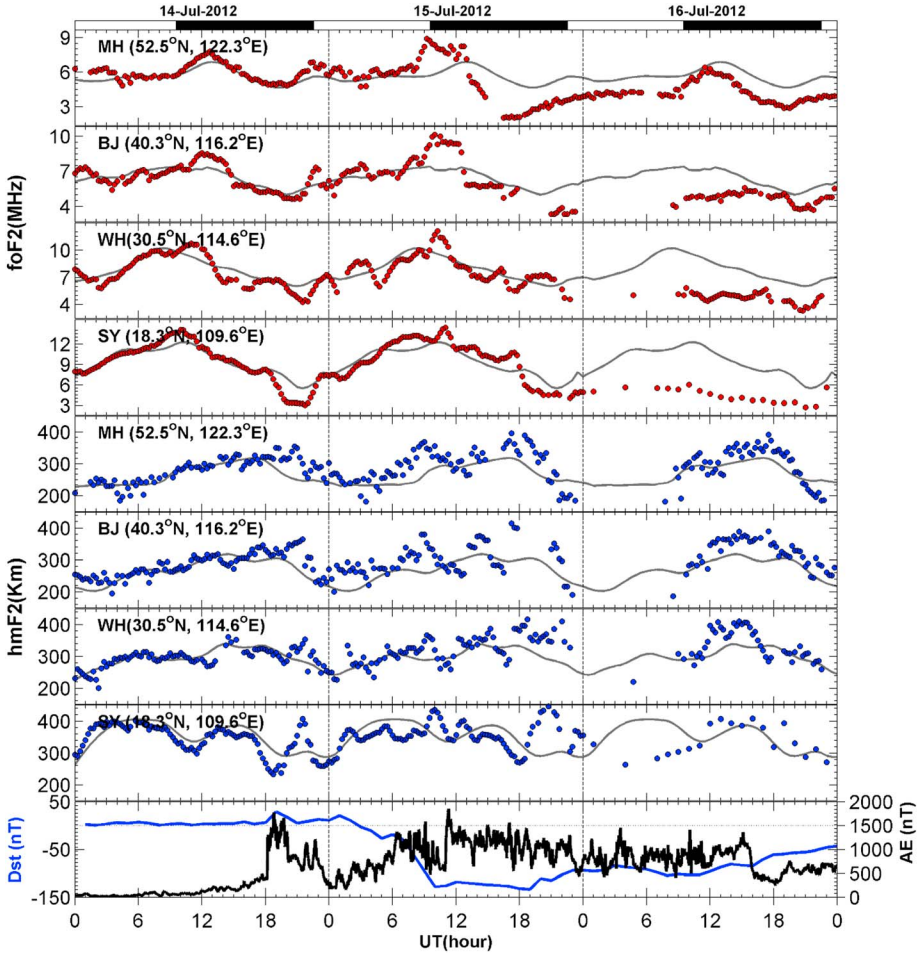

Figure 3. Variations of f_oF_2 and h_mF_2 at station MH, BJ, WH, and SY on 14–17 July 2013. The gray lines represent the reference values on 13 July 2012. The *Dst* and *AE* indices at the bottom panel are used to characterize the evolution of geomagnetic storm.

peak excursions of h_mF_2, we can infer that the propagation time from the MH to SY is about 2 h and the distance between them is about 4200 km. The propagation speed of this disturbance is ~590 m/s, which matches the characteristics of large-scale traveling ionospheric disturbances (LSTIDs). LSTIDs with horizontal velocities between 400 and 1000 m/s and periods in the range of 30 min to 3 h [e.g., *Afraimovich et al*., 2002; *Lee et al*., 2004; *Ding et al*., 2007] may be generated during storms or substorms as a result of large amount of energy deposition in the high latitudes [e.g., *Lu et al*., 2001]. They propagated from high to low latitudes with reduced amplitudes due to ion drag dissipations and showed time delays at different sites along the propagation direction of LSTIDs [e.g., *Hunsucker*, 1982; *Hocke and Schlegel*, 1996]. In addition, f_oF_2 and h_mF_2 exhibited not in phase correlations as observed in these four sites during the passage of LSTIDs. For example, the most pronounced peak of f_oF_2 on 15 July lagged behind that of h_mF_2 for about 1 h over these sites. The phase correlations between f_oF_2 and h_mF_2 have been investigated in depth from both observations and theoretical analyses [e.g., *Prölss and Jung*, 1978; *Fesen et al*., 1989; *Bauske and Prölss*, 1997; *Lu et al*., 2001; *Lee et al*., 2004; *Lei et al*., 2008]. *Bauske and Prölss* [1997] simulated the ionospheric f_oF_2 and h_mF_2 variations at middle latitudes during the passage of Travelling Atmospheric Disturbance (TAD) and revealed that h_mF_2 was elevated and a decrease in N_mF_2 in the initial phase. However, both h_mF_2 and N_mF_2 increased in the recovery process. According to their simulation results, the initial negative correlation between them is shorter in duration and N_mF_2 is weaker in magnitude in the initial phase relative to them in the recovery phase. As a result, the negative correlation between them at middle latitudes may be masked in the initial phase but N_mF_2 enhancement is preceded by increase in h_mF_2.

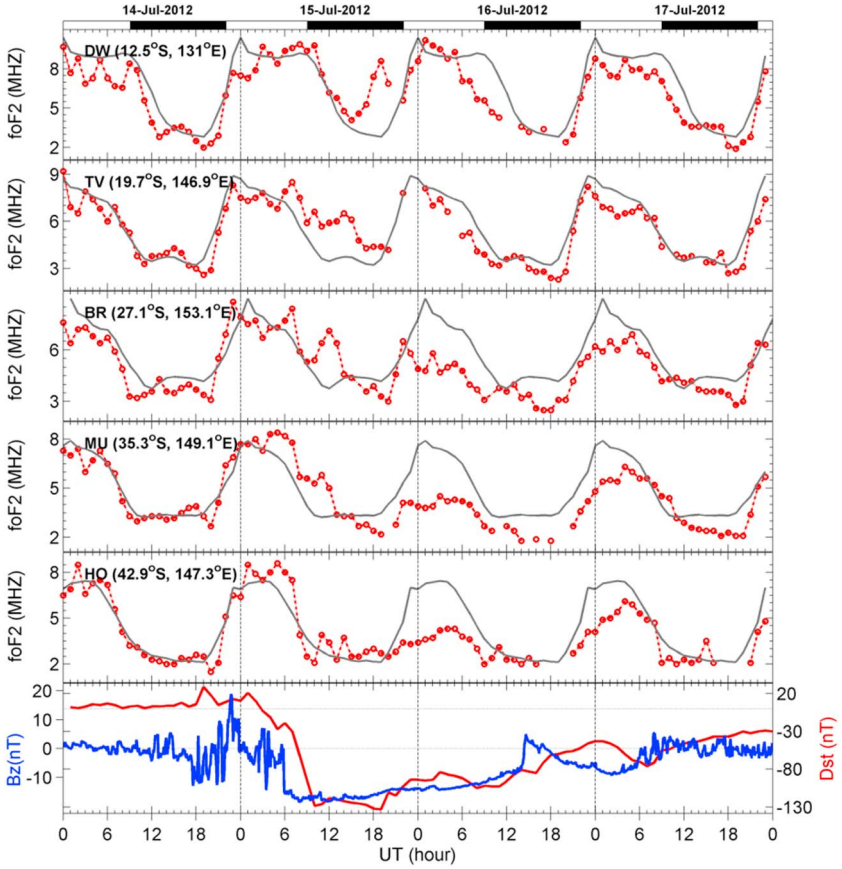

Figure 4. Variations of f_oF_2 at sites DW, TV, BR, MU, and HO on 14–17 July 2013. The gray lines represent the reference values on 13 July 2012.

As shown in Figure 4, f_oF_2 enhancements during 0100–1000 UT 15 July over all the five sites in the Southern Hemisphere took place in the main phase and were delayed at lower latitudes, suggesting the disturbed wind field effects which were associated with the major *AE* intensification in the initial phase. For a perspective of equatorial electrodynamical information, Figure 5 showed that the equatorial electric electrojet (EEJ) over East Asia was weakened during 0000–0700 UT 15 July, indicating that the DDEF could be active during this interval. Spiky like changes were superposed in the EEJ curve which were most probably caused by the existence of short-lived PPEF in an environment of DDEF since IMF B_z had a rapid changes in its directions during this interval. Taken the above the phenomena into consideration, we were in a good position to explain the latitudinal variation of TEC in Figure 2. Storm-generated equatorward winds, which typically lag behind the enhanced auroral energy input, lifted the ionosphere at middle and low latitudes to higher altitudes with reduced recombination and corresponding increment in TEC of both hemispheres [e.g., *Lu et al*., 2012]. In low-equatorial regions, DDEF may play a part in the evolvement of TEC evidenced by the decreased dayside eastward EEJ strength. Under its effects, a weakened fountain effects took place and resulted in a decrease of TEC in the EIA crest regions and an increase in TEC over the equator.

3.2.2. Long-Lived Westward Equatorial Electrojet and Inhibition of EIA in the Recovery Phase

It is illustrated in Figure 2 that daytime EIA crest in the Northern Hemisphere was severely inhibited and DTEC presented a remarkable decrease with the maximum amplitude of ~25 TECU on 16 July. In the Southern Hemisphere, negative phase of TEC at low latitudes prevailed almost the entire day of the 16 July, which was weaker than that in the summer hemisphere. Long-term depression of f_oF_2 at MH, NJ, WH, and SY coincided with the negative phase of TEC. On the dayside of 16 July, the ionospheric F_2 layers at these four sites were lowered and this tendency became reversed at night. In the Australian sector, the negative phase was more appreciable at higher latitudes on the same day. The strong negative ionospheric storm effects will be interpreted later.

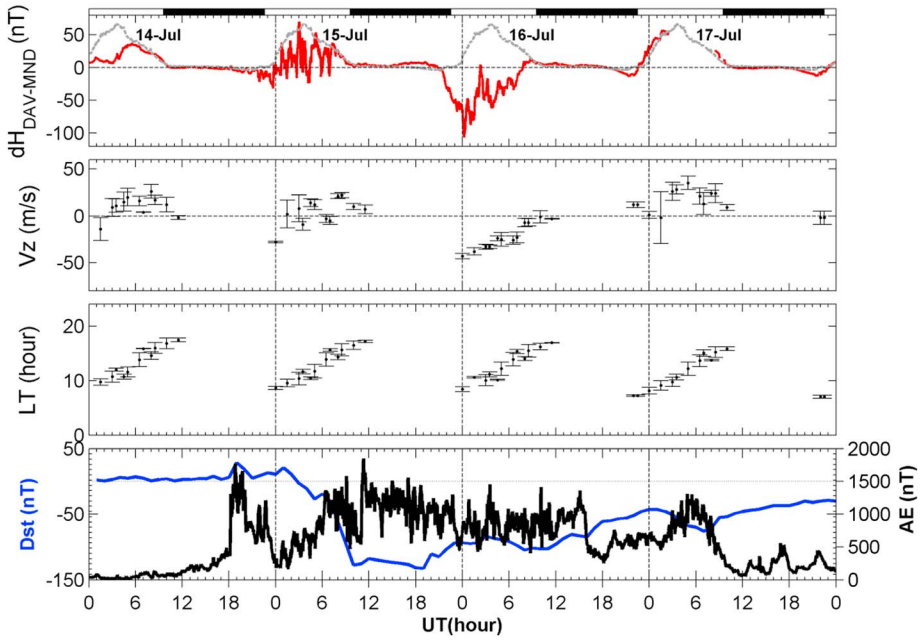

Figure 5. From the top to the bottom are the $dH_{DAV\text{-}MND}$ (difference between the *H* horizontal component at equator DAV and nonequator station MND), plasma vertical drift around dip equator in Asian-Australian sector (in the geographic longitude range [80°–140°]) observed by C/NOFS, local time of the C/NOFS observations, and *Dst* and *AE* indices. The dashed gray line in the top panel denotes the reference value on 13 July. The error bars in the second and third panels stand for the standard deviations.

It is shown in Figure 5 that westward electrojet with peak excursion of ~ −100 nT took place almost the entire daytime on 16 July. C/NOFS measured vertical drifts have also revealed that strong downward drift occurred around the dip equator on the dayside. This has implications in that westward electric fields appear in this interval. The comparison between the $dH_{DAV\text{-}MND}$ and C/NOFS vertical drifts demonstrated the reliability of our drift estimated by C/NOFS IVM during geomagnetic storms. *Rodrigues et al*. [2011] compared IVM-measured vertical drift with Jicamarca incoherent scatter radar drift measurements and found a good agreement between them in capturing the characteristics of equatorial electric fields during sudden stratospheric warming event. The agreement between the two different approaches during geomagnetic storms was also quite satisfactory in capturing the long-lived ionospheric disturbed electric field. The most likely candidate of westward electrojet here was DDEF, which typically has a westward polarity at the daytime and occurs often with time scales of several to dozens of hours after larger energy dissipations into the high latitudes [*Scherliess and Fejer*, 1997].

3.3. Main Features of Ionospheric Disturbances in the American Sector

3.3.1. Appearance of SED in the Northern Summer Hemisphere in the Initial Phase

Figure 6 illustrates that prominent plume-like enhancements with the maximum increment of ~ 20 TECU extending from high to low latitudes were shown around the dusksides at 00:00–05:00 UT on 15 July in the North American, persisting for about 5 h. Two-dimensional GPS TEC maps have indicated a typical storm-enhanced density (SED) event (not shown here). It was thought that there are two steps in forming the SED phenomena including electron density enhancement at and poleward of EIA crest regions associated with plasma uplift and redistribution from low to middle latitudes caused by PPEF and then sunward and poleward convection of the elevated TEC plume [*Foster*, 1993; *Kelley et al*., 2004]. Figure 7 depicts the EEJ in the American longitude (Figure 7a), h_mF_2 (Figure 7b), and f_oF_2 (Figure 7c) measured by Jicamarca ionosonde (LT = UT − 5) and *Dst* and *AE* indices (Figure 7d). In Figure 7a, there is a good agreement between $dH_{HUA\text{-}KOU}$ (red line) and $dH_{JIC\text{-}PIU}$ (blue line) in capturing the daytime EEJ on 14 July giving us the confidence that using $dH_{HUA\text{-}KOU}$ as a replacement in the presence of data gap in $dH_{JIC\text{-}PIU}$. Prior to the dramatic TEC increment, IMF turned southward and consequently *AE* intensification during 1600–1800 UT on 14 July. The daytime EEJ on 14 July was also stronger than the reference day. The long-term increased EEJ over the

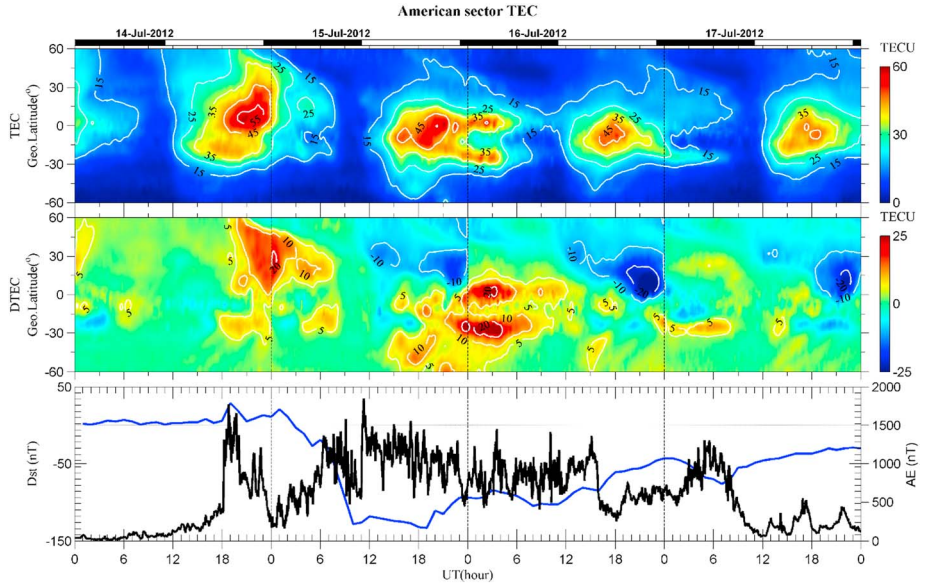

Figure 6. TEC and the deviations of TEC with respect to the value of 13 July derived from GPS network in the American sector (~70°E) on 14–17 July 2012.

equatorial ionosphere was analogous to the phenomenon reported by *Huang et al.* [2007] in which the equatorial ionospheric electric fields was enhanced for 2.5 h as a consequence of long-duration of PPEF due to weak southward component IMF B_z (~4 nT) during 1442–1712 UT on 23 September 2002. Later on, a short-lived change was superimposed on the EEJ curve at around 1800 UT in accompany with *AE* intensification indicating the role of PPEF. At the same time, the equatorial ionosphere over Jicamarca was elevated by several tens of kilometers. It seems that the enhanced eastward ionospheric fields have played a role in the

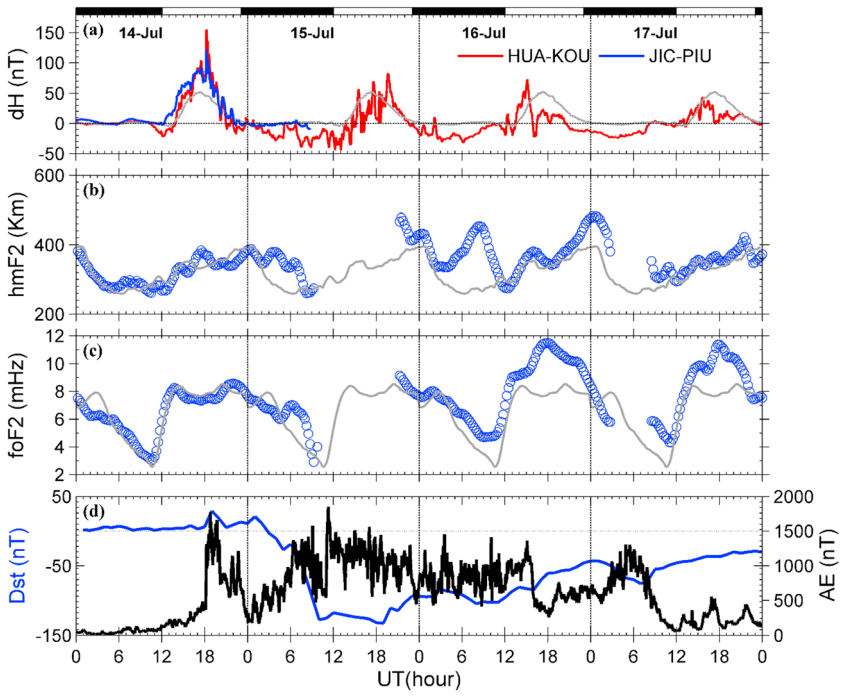

Figure 7. (a) $dH_{HUA\text{-}KOU}$ and $dH_{JIC\text{-}PIU}$. (b and c) h_mF_2 and f_oF_2 at Jicamarca (LT = UT − 5). (d) *Dst* and *AE* indices. The gray line in Figure 7a denotes the reference value of $dH_{HUA\text{-}KOU}$ on 13 July.

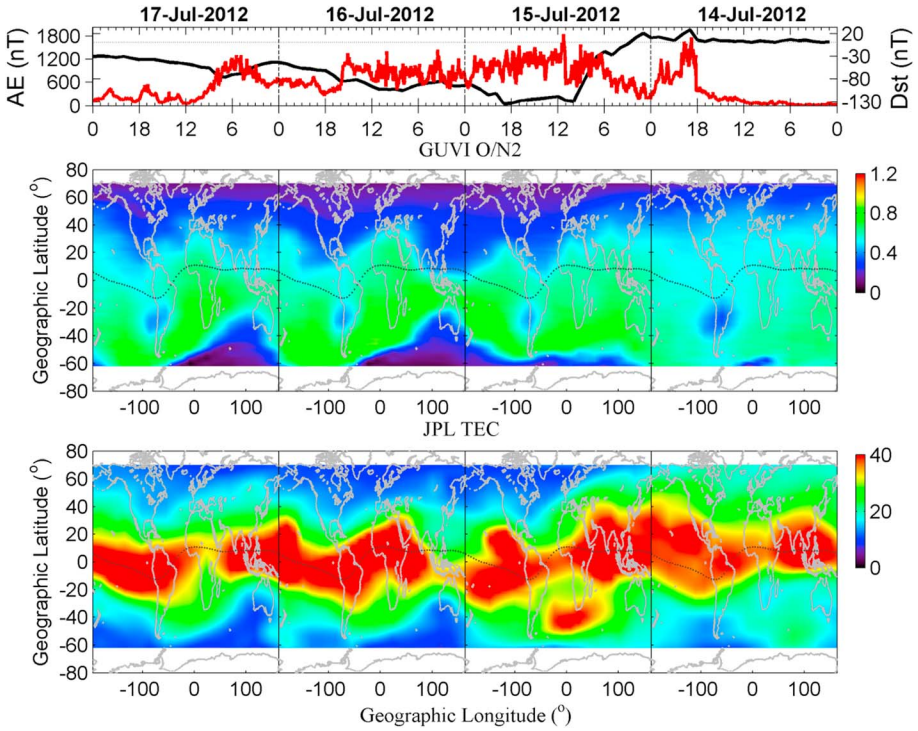

Figure 8. (top) *Dst* and *AE* indices, (middle) TIMED/GUVI O/N_2 ratio, and (bottom) Jet Propulsion Laboratory (JPL)-provided composite TEC (in units of TECU) on 14–17 July 2012. Time runs from right to left, and O/N_2 from consecutive TIMED orbits are superposed on the geographic latitude and longitude.

TEC enhancement at middle and low latitudes through providing additional plasmas and uplifting the ionosphere. Thermospheric wind during storm conditions may also play very important role in increasing TEC in the American sector as the simulation results by *Sojka et al*. [2012].

3.3.2. Periodical Intrusion of Negative Phase and Nighttime EIA Intensifications in the Recovery Phase

As illustrated in Figure 6, an intriguing feature is seen in the Northern Summer Hemisphere following the SED phenomenon. Negative ionospheric storm effects appeared in the Northern Hemisphere on 15 July, commenced at higher latitudes in the postmidnight sector, propagated toward low latitudes, and terminated in the dusk sector. The negative phase front approached the geographic equator. The TEC negative phase in the following 2 days resembled manners of that on 15 July regarding its temporal and spatial evolvements. The depletion of TEC at low latitudes mainly occurred in the Northern Summer Hemisphere but almost disappeared in the Southern Winter Hemisphere.

As we know, there is a close association between electron density variations and neutral composition changes during geomagnetic storms. Figure 8 displays *Dst* and *AE* indices (top), TIMED/GUVI O/N_2 ratio (middle), and Jet Propulsion Laboratory (JPL) composite TEC (in units of TECU, bottom) on 14–17 July 2012. TEC provided by JPL are projected onto the TIMED orbits. Note that time runs from right to left. As storm progressed, the depleted O/N_2 region ($O/N_2 < \sim 0.4$) expanded toward lower latitudes and exhibited hemispheric asymmetry. The low O/N_2 ratio regions reached the dip equator in the Northern Summer Hemisphere, while they only reached 20° in the Southern Winter Hemisphere during 0000–0600 UT on 16 July.

Besides the pronounced depletion of TEC at high and middle latitudes, salient increment of TEC is also shown at low latitude of both hemispheres on the nightside on 16 July in Figure 6. The EIA crest regions started to increase at ~ 2300 UT on 15 July and diminished at ~1200 UT on 16 July. It is depicted in Figure 6 that TEC at low latitudes started to increase in the afternoon sector on 15 July and lasted almost the entire night of 16 July with stronger increments around EIA crests than in the trough region. The EIA structure persisted from the dayside to the postmidnight sector on 16 July. At this time, the equatorial ionosphere was significantly elevated over Jicamarca. For example, in Figure 7, h_mF_2 was increased by about 200 km from ~280 km to ~480 km. $dH_{DAV\text{-}MND}$ in the East Asia depicted in Figure 5 that long-term westward EEJ sustaining about 24 h was developed from

2200 UT 15 July to 0800 UT 16 July, peaking around 2400 UT 15 July. As discussed before, the most likely candidate for this westward is DDEF, which is the generally westward on the nightside and eastward on the dayside. Thus, it is not surprised to see that the uplift of ionosphere in the nighttime American longitude, which should be due to the effects of nighttime eastward DDEF.

4. Discussion

4.1. Oscillations of Negative Ionospheric Storm Effects at Low Latitudes

In the American sector, remarkable daytime TEC depletions were seen at low latitudes for three consecutive days. As shown in Figure 8, high- to middle-latitude ionosphere was immersed in the neutral composition disturbance zone during 15–17 July. A strong negative phase storm also occurred at low latitudes on 16 July 2000 great geomagnetic storm and the G-condition in the ionograms was clearly seen on the early first day this geomagnetic storm [e.g., *Liu et al*., 2002]. They ascribed this negative ionospheric phase to the effects of neutral composition changes. It is generally accepted that the negative ionospheric phase should be attributed to the changes in the thermospheric composition due to the heating of the thermosphere during the geomagnetic storms since the first suggestion from *Seaton* [1956]. It is depicted in Figure 8 that the negative storm phase was well correlated to the neutral composition disturbance area. As presented by *Prölss* [1995] and *Fuller-Rowell et al*. [1994], the neutral composition area equatorward expansion preferably commences in the early morning sector and has a preference for the longitudes where the magnetic poles locate. Thus, the composition change effects are more profound in the North American where the north magnetic pole locates. As shown in Figure 6, the negative storm phase recurred for three consecutive days in the American longitude extended from auroral region to the midlatitudes in the early morning and reached the lowest latitude in the duskside as a result of the gradual recovery of neutral composition disturbance in the daytime. The scalloping effects of TEC in the American longitude were mainly caused by intrusion of neutral composition disturbance zone driven by everlasting enhanced auroral geomagnetic activity. It was supported by the fact that the *AE* index is large (~1000 nT) during 0600 UT 15 July to 1600 UT 16 July and 0400 UT–0800 UT 17 July. The prolonged southward IMF B_z component allowed the solar wind energy input into the atmosphere continuously and consequent neutral composition disturbances. The neutral composition disturbance did not recover completely due to continuous auroral energy dissipations. Statistical study revealed that repeated occurrences of positive and negative disturbances every 24 h or so during the recovery phase have been detected in European middle latitudes [e.g., *Stankov et al*., 2010]. *Kutiev et al*. [2005] also found a similar phenomenon in which an oscillation-like alternation of positive and negative disturbances in GPS TEC in East Asia with a period of 24 h was observed during a 4 day moderate geomagnetic storm. They ascribed the observed oscillation-like behavior to the alternative change in the atmospheric circulation, resulting in the upward and downward movement of the equatorial ionosphere.

It is illustrated in Figure 2 that the negative phase of TEC was also predominant in the East Asian sector in the recovery phase. The daytime EIA was severely inhibited, and the northern EIA crest disappeared on 16 July. f_oF_2 over Sanya was depressed to the lowest level during the recent 2 years. It is demonstrated in Figure 8 that the neutral composition disturbance zone ($O/N_2 < 0.4$) had expanded to the dip equator in the Summer Hemisphere at 0000–0600 UT 16 July, indicating the important role of O/N_2 in decreasing electron density in the EIA northern crest regions. It is shown in Figure 8 that the composition disturbance area expanded to the dip equator in the Northern Hemisphere but only reached the ~25°S at ~0200 UT 16 July. As summarized by *Liu et al*. [2012a], combined effects of uneven auroral energy input and prevailing background summer-to-winter winds contribute to the seasonal asymmetry of neutral composition disturbances and in turn modify plasma chemical reactions. Larger thermospheric heating rate in the summer hemisphere tend to disturb the neutral atmosphere to a greater extent. Difference in thermospheric background wind is an important factor contributing to summer-winter difference in the neutral atmosphere response. The zonal mean meridional wind driven by differential solar heating is generally from the summer to winter. The disturbance-driven circulation is equatorward in both hemispheres. The prevailing summer-to-winter zonal mean solar-driven circulation tends to facilitate the equatorward expansion of the density disturbance in the summer hemisphere and restrict its expansion in the winter hemisphere. Therefore, combined effects of uneven auroral energy input and asymmetry in background neutral winds are more favorable for the neutral composition zone expansion in the summer

hemisphere than in the winter hemisphere. The prevailing summer-to-winter transequatorial winds tend to transport the plasmas from the upwind hemisphere to the downwind hemisphere and increase/decrease the electron content in the downwind/upwind hemisphere, leading to the hemispheric asymmetry as shown in Figure 6 from 2300 UT 15 July to 0800 UT 16 July.

The equatorial boundary of O/N_2 disturbance area was only close to ~ −30° geographic latitude far from the normal southern crest region, but TEC decreased over this region, suggesting that other physical processes should be responsible for the negative ionospheric storm effects on the EIA area apart from the neutral composition changes. The long-term westward EEJ over the equator could be another important resource for the negative storm phase. The duration and direction of the daytime westward EEJ match the features of DDEF, which is typically westward on the nightside and eastward on the dayside [*Fejer and Scherliess*, 1997]. Under the effects of DDEF, an inverted fountain took place, the daytime East Asian EIA was inhibited, and the ionospheric *F* region over Sanya was depressed to a very low altitude. The conditions in the opposite longitude sector were depicted in Figure 6 that TEC at low latitudes was increased in the nightside sector on 16 July and lasted almost the entire night of 16 July with stronger increments around EIA crests than in the trough region. The EIA structure persisted from the dayside to the postmidnight sector on 16 July. At this time, the equatorial ionosphere was significantly elevated over Jicamarca. The maximum increase in h_mF_2 was about 200 km from ~280 km to ~480 km. $dH_{DAV\text{-}MND}$ in the East Asian showed that long-term westward EEJ sustaining about 24 h was developed and started from 2200 UT 15 July to 0800 UT 16 July, peaking around 2400 UT 15 July. Therefore, the negative storm effects on TEC in the southern EIA crest regions were only caused by the daytime westward DDEF effects, but both O/N_2 changes and DDEF effects were important in decreasing TEC in the Northern Hemisphere EIA crest regions.

4.2. Strengthened EIA by the Multiple Undershielding PPEF

The long-term westward daytime EEJ in the East Asia imply that DDEF were operative during the interval 2300 UT 15 July to 0800 UT 16 July. In general, the DDEF over the dip equator is westward on the dayside and eastward on the nightside. According to the statistical results and numerical outcomes, the local time of reversal of the equatorial zonal perturbation electric fields has 2–3 h variability and reversal of DDEF from west to east is after prereversal enhancement at about 2130–2400 LT depending on the geomagnetic storm intensity, longitude, season, and solar activity [*Huang*, 2005; *Fejer et al*., 2008]. As a result, the westward DDEF typically reduces the prereversal enhancement of equatorial *F* layer vertical drift and suppresses the formation of postsunset EIA [e.g., *Sobral et al*., 2001; *Zhao et al*., 2008]. However, this does not agree with current situation because the nighttime EIA was enhanced and expanded to higher latitudes from 2300 UT/1800 LT 15 July to 0800 UT/0300 LT 16 July in Figure 6. The double crest enhancements were more than 20 TECU and exhibited hemispheric difference with more evident increments in the Southern Hemisphere. h_mF_2 over Jicamarca started to increase at ~ 0200 UT/2100 LT 16 July, reached the maximum ~520 km at 0800 UT/0300 LT, and recovered to the prestorm level at 1100 UT/0600 LT. The significant uplift of equatorial ionosphere revealed the existence of eastward electric field around sunset.

The most plausible cause responsible for equatorial ionosphere F_2 region uplift for ~120 km at 2136 UT and simultaneous EIA enhancement on the daytime and around sunset is the eastward penetration electric fields. There were several sharp and short-lived changes in the equatorial EEJ when the IMF B_z was stable southward and solar wind dynamic pressure changed smoothly. It is shown in Figure 9 that three spikes higher than quiet vales in the $dH_{HAU\text{-}KOU}$ curves were seen at 1532 UT, 1736 UT, and 1939 UT on 15 July. The fourth one enhancing westward EEJ can be identified from the $dH_{DAV\text{-}MND}$ curve at 0017 UT on 16 July and is expected to be eastward at ~1900 LT. And also, there is no way to exclude the possibility of stronger prereversal enhancement on this day than that on the reference day due to ionospheric day-to-day variability which is possibly related to the upward propagating effects of gravity waves, tides, planetary waves, or irregular winds in the dynamo region other than geomagnetic storm sources.

Considerable structure is presented in the *AE* index, and it appears that multiple substorms occurring as indicated in Figure 9. Interactions between PPEF and DDEF add the relationship complexity between substorms and PPEF effects on EEJ [*Maruyama et al*., 2005]. A series of substorms may be in progress at storm times as indicated by the strong auroral activity during stable southward IMF B_z intervals 0700 UT 15 July to 1600 UT 16 July. There is a controversy regarding to the direction of PPEF triggered by substorms.

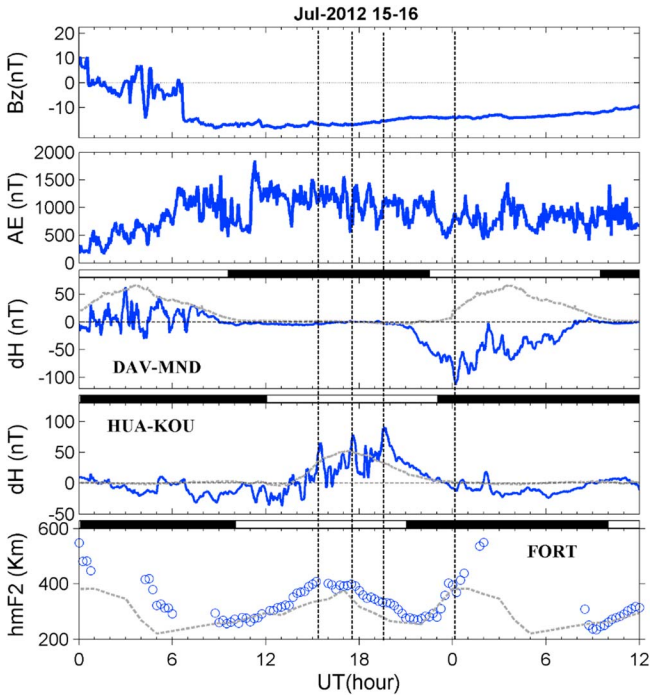

Figure 9. From the top to the bottom are IMF B_z, *AE* indices, $dH_{DAV\text{-}MND}$, $dH_{HUA\text{-}KOU}$, and h_mF_2 over Fortaleza on 15–16 July 2012.

Some of case studies supported the existence of westward perturbed electric field on the dayside [e.g., *Fejer et al*., 1979; *Kikuchi et al*., 2000; *Wei et al*., 2009] based on the arguments that convection electric field decreases abruptly or region 2 (R2) field-aligned currents (FACs) increase suddenly during substorms. Other observational evidences supported the opposite conclusions that the substorms-related PPEF are eastward [*Huang et al*., 2004; *Zhao et al*., 2005]. This event conforms to the later results. The deduction of the reason responsible for the dayside eastward PPEF is quite difficult since it requires a comprehensive knowledge of inner magnetosphere dynamics during disturbed conditions. Only a tentative explanation is given here. PPEF occurs during periods of temporary imbalance between the dawn-dusk penetrating convection electric field related to region 1 (R1) FACs and dusk-dawn shielding electric field in association with R2 FACs. R2 FACs flowing up from the dawnside ionosphere near plasma sheet inner edge and downward into the duskside take longer time to balance the enhanced/decreased region 1 FACs since it takes time for the inner edge of plasma sheet to readjust to a change in convection. The inner edge of the plasma sheet tends to shield the inner-Earth region from the dawn-dusk convection field. A succession of substorms may take place when the IMF B_z is strongly southward for an extended period and result in the collapse of cross-tail current near the inner edge of plasma sheet. The disappearance of cross-tail current during substorm expansive phase contributes to the breakdown in shielding the inner magnetosphere from the dawn-dusk convection electric field [*Rostoker*, 1996; *Wolf et al*., 2007], leading to the eastward daytime PPEF. In addition, the shielding effects vary with plasma sheet condition and the shielding efficiency is higher when the plasma sheet is cold and dense [e.g., *Spiro et al*., 1988; *Richmond et al*., 2003]. During the substorm expansion phase the plasma sheet will be heated [*Baumjohann et al*., 1996] and resultant shielding electric field reduction.

During 0100 UT–0300 UT 16 July, the ionospheric *F* layer over Jicamarca recovered to normal quiet time position and raised again after that, implying the reversal of DDEF from westward to eastward at around 2200 LT. After the reversal of DDEF direction, from westward to eastward, the fountain effect is enhanced, which tends to move the *F* region upward in the equatorial ionosphere, at the same time that ionization is transported to higher latitudes, giving rise to decrease in f_oF_2 and uplift of the equatorial ionosphere. The slight enhanced f_oF_2 over the equator is most possibly related to the increased O/N_2 due to the convergence of thermospheric circulations.

h_mF_2 at Jicamarca exhibits a large increase at around 0300 UT (~2200 LT) on 16 July (Figure 7), while at Fortaleza similar increase start happens at 0000 UT (~2230 LT) on 16 July (Figure 9). Both stations are in the equatorial anomaly trough, with Fortaleza being about 2.5 h ahead. Our current results are in consistent with reversal local time of DDEF directions as obtained from observations and model simulation outcomes [e.g., *Richmond et al*., 2003; *Huang et al*., 2005; *Fejer et al*., 2008]. Similar phenomena relating to the nighttime height increase beginning over Fortaleza prior to it over Jicamarca by about 3 h is also observed during 21–22 January 2005 storm [*Santos et al*., 2012]. They pointed out that the DDEF effects were more remarkable over Jicamarca than Fortaleza and attributed the difference to the presence of local time dependence.

5. Conclusion

We have analyzed the ionospheric and thermospheric responses to a geomagnetic storm event triggered by unusual prolonged southward IMF B_z, using the multidata resources in the American sector and the East Asian sector on 14–17 July 2012. The main conclusions are listed as follows:

1. Long-term and strong depressions of ionospheric TEC and f_oF_2 over the East Asian longitudes appeared in the recovery phase caused by neutral composition changes and more than 24 h DDEF effects. The negative ionospheric phase in the American sector recurred with 24 h period for three consecutive days.
2. Multiple PPEF occur when the IMF B_z was stable southward and dynamic pressure was also steady. The nighttime equatorial ionosphere over Jicamarca was elevated for ~200 km under the combined effects of PPEF and DDEF which were also responsible for the nighttime enhanced EIA.
3. The ionospheric f_oF_2 enhancement caused by TIDs was delayed for about an hour with respect to the increase in h_mF_2.
4. Strong longitudinal/UT difference in the ionosphere response over Fortaleza (Brazil) and Jicamarca (Peru) in terms of the onset of nighttime upward drifts is readily explained by the local time dependence of DDEF.

Acknowledgments

The authors are indebted to the accessible to these databases used in this work. GPS TEC data are provided by the MIT Haystack Observatory Madrigal database (http://www.openmadrigal.org) and Jet Propulsion Laboratory. We are grateful of the Center for Atmospheric Research, University of Massachusetts Lowell, for providing the ionogram data of Debase. This research was supported by the Chinese Academy of Sciences (KZZD-EW-01-3), the National Key Basic Research Program of China (2012CB825604), National Natural Science Foundation 41321003 of China (41174065 and 41304128), and China Postdoctoral Science Foundation. This work was supported by International Exchange Program of National Institute of Information and Communications (NICT).

Michael Liemohn thanks Alexey Danilov and Ivan Kutiev for their assistance in evaluating this paper.

References

Afraimovich, E. L., et al. (2002), Simultaneous radio and optical observations of the mid-latitude atmospheric response to a major geomagnetic storm of 6–8 April 2000, *J. Atmos. Sol. Terr. Phys.*, *64*, 1943–1955.

Anderson, D., A. Anghel, K. Yumoto, M. Ishitsuka, and E. Kudeki (2002), Estimating daytime vertical E×B drift velocities in the equatorial F-region using ground-based magnetometer observations, *Geophys. Res. Lett.*, *29*(12), 1596, doi:10.1029/2001GL014562.

Balan, N., Y. Otsuka, M. Nishioka, J. Y. Liu, and G. J. Bailey (2013), Physical mechanisms of the ionospheric storms at equatorial and higher latitudes during the recovery phase of geomagnetic storms, *J. Geophys. Res. Space Physics*, *118*, 2660–2669, doi:10.1002/jgra.50275.

Baumjohann, W., Y. Kamide, and R. Nakamura (1996), Substorms, storms, and the near-Earth tail, *J. Geomagn. Geoelectr.*, *48*, 177–185.

Bauske, R., and G. W. Prölss (1997), Modeling the ionospheric response to traveling atmospheric disturbances, *J. Geophys. Res.*, *102*, 14,555–14,562, doi:10.1029/97JA00941.

Blanc, M., and A. D. Richmond (1980), The ionospheric disturbance dynamo, *J. Geophys. Res.*, *85*, 1669–1686, doi:10.1029/JA085iA04p01669.

Buonsanto, M. J. (1999), Ionospheric storms: A review, *Space Sci. Rev.*, *88*, 563–601.

Burns, A. G., T. L. Killeen, and R. G. Roble (1989), Processes responsible for the compositional structure of the thermosphere, *J. Geophys. Res.*, *94*(A4), 3670–3686, doi:10.1029/JA094iA04p03670.

Christensen, A. B., et al. (2003), Initial observations with the Global Ultraviolet Imager (GUVI) in the NASA TIMED satellite mission, *J. Geophys. Res.*, *108*(A12), 1451, doi:10.1029/2003JA009918.

Danilov, A. D. (2001), F2-region response to geomagnetic disturbances, *J. Atmos. Sol. Terr. Phys.*, *63*, 441–449.

Danilov, A. D. (2013), Ionospheric F-region response to geomagnetic disturbances, *Adv. Space Res.*, *52*(3), 343–366, doi:10.1016/j.asr.2013.04.019.

Ding, F., W. Wan, B. Ning, and M. Wang (2007), Large-scale traveling ionospheric disturbances observed by GPS total electron content during the magnetic storm of 29–30 October 2003, *J. Geophys. Res.*, *112*, A06309, doi:10.1029/2006JA012013.

Fejer, B. G. (2011), Low latitude ionospheric electrodynamics, *Space Sci. Rev.*, *158*, 145–166, doi:10.1007/s11214-010-9690-7.

Fejer, B. G., and L. Scherliess (1995), Time dependent response of equatorial ionospheric electric fields to magnetospheric disturbances, *Geophys. Res. Lett.*, *22*, 815–854.

Fejer, B. G., and L. Scherliess (1997), Empirical models of storm time equatorial zonal electric fields, *J. Geophys. Res.*, *102*(A11), 24,047–24,056, doi:10.1029/97JA02164.

Fejer, B. G., C. A. Gonzalez, D. T. Farley, and M. C. Kelly (1979), Equatorial electric fields during magnetically disturbed conditions: 1. The effect of the interplanetary magnetic field, *J. Geophys. Res.*, *84*, 5797–5802, doi:10.1029/JA084iA10p05797.

Fejer, B. G., J. W. Jensen, and S.-Y. Su (2008), Seasonal and longitudinal dependence of equatorial disturbance vertical plasma drifts, *Geophys. Res. Lett.*, *35*, L20106, doi:10.1029/2008GL035584.

Fesen, C. G., G. Growley, and R. G. Roble (1989), Ionospheric effects at low latitudes during the March 22, 1979, geomagnetic storm, *J. Geophys. Res.*, *94*, 5405–5417, doi:10.1029/JA094iA05p05405.

Foster, J. C. (1993), Storm time plasma transport at middle and high latitudes, *J. Geophys. Res.*, *98*, 1675–1690, doi:10.1029/92JA02032.

Fuller-Rowell, T. J., M. V. Codrescu, R. J. Moffett, and S. Quegan (1994), Response of the thermosphere and ionosphere and geomagnetic storms, *J. Geophys. Res.*, *99*, 3893–3914, doi:10.1029/93JA02015.

Guo, J., X. Feng, P. Zuo, J. Zhang, Y. Wei, and Q. Zong (2010), Interplanetary drivers of ionospheric prompt penetration electric fields, *J. Atmos. Sol. Terr. Phys.*, doi:10.1016/j.jastp.2010.01.010.

Hocke, K., and K. Schlegel (1996), A review of atmospheric gravity waves and travelling ionospheric disturbances: 1982–1995, *Ann. Geophys.*, *14*, 917.

Huang, C.-S., J. C. Foster, L. P. Goncharenko, G. D. Reeves, J. L. Chau, K. Yumoto, and K. Kitamura (2004), Variations of low-latitude geomagnetic fields and Dst index caused by magnetospheric substorms, *J. Geophys. Res.*, *109*, A05219, doi:10.1029/2003JA010334.

Huang, C.-S., J. C. Foster, and M. C. Kelley (2005a), Long-duration penetration of the interplanetary electric field to the low-latitude ionosphere during the main phase of magnetic storms, *J. Geophys. Res.*, *110*, A11309, doi:10.1029/2005JA011202.

Huang, C. M., A. D. Richmond, and M. Q. Chen (2005b), Theoretical effects of geomagnetic activity on low-latitude ionospheric electric fields, *J. Geophys. Res.*, *110*, A05312, doi:10.1029/2004JA010994.

Huang, C.-S., S. Sazykin, J. L. Chau, N. Maruyama, and M. C. Kelley (2007), Penetration electric fields: Efficiency and characteristic time scale, *J. Atmos. Terr. Phys.*, *69*(10–11), 1135–1146.

Hunsucker, R. D. (1982), Atmospheric gravity waves generated in the high latitude ionosphere: A review, *Rev. Geophys.*, *20*, 293–315, doi:10.1029/RG020i002p00293.

Kelley, M. C., J. J. Makela, J. L. Chau, and M. J. Nicolls (2003), Penetration of the solar wind electric field into the magnetosphere/ionosphere system, *Geophys. Res. Lett.*, *30*(4), 1158, doi:10.1029/2002GL016321.

Kelley, M. C., M. N. Vlasov, J. C. Foster, and A. J. Coster (2004), A quantitative explanation for the phenomenon known as storm-enhanced density, *Geophys. Res. Lett.*, *31*, L19809, doi:10.1029/2004GL020875.

Kikuchi, T., H. Liihr, K. Schlegel, H. Tachihara, M. Shinohara, and T.-I. Kitamura (2000), Penetration of auroral electric fields to the equator during a substorm, *J. Geophys. Res.*, *105*(A10), 23,251–23, 261, doi:10.1029/2000JA900016.

Kutiev, I., S. Watanabe, Y. Otsuka, and A. Saito (2005), Total electron content behavior over Japan during geomagnetic storms, *J. Geophys. Res.*, *110*, A01308, doi:10.1029/2004JA010586.

Lee, C. C., J. Y. Liu, M. Q. Chen, S. Y. Su, H. C. Yeh, and K. Nozaki (2004), Observation and model comparisons of the traveling atmospheric disturbances over the Western Pacific region during the 6–7 April 2000 magnetic storm, *J. Geophys. Res.*, *109*, A09309, doi:10.1029/2003JA010267.

Lei, J., A. G. Burns, T. Tsugawa, W. Wang, S. C. Solomon, and M. Wiltberger (2008), Observations and simulations of quasiperiodic ionospheric oscillations and large-scale traveling ionospheric disturbances during the December 2006 geomagnetic storm, *J. Geophys. Res.*, *113*, A06310, doi:10.1029/2008JA013090.

Li, G., et al. (2010), Longitudinal development of low-latitude ionospheric irregularities during the geomagnetic storms of July 2004, *J. Geophys. Res.*, *115*, A04304, doi:10.1029/2009JA014830.

Lin, C. H., A. D. Richmond, R. A. Heelis, G. J. Bailey, G. Lu, J. Y. Liu, H. C. Yeh, and S.-Y. Su (2005), Theoretical study of the low- and midlatitude ionospheric electron density enhancement during the October 2003 superstorm: Relative importance of the neutral wind and the electric field, *J. Geophys. Res.*, *110*, A12312, doi:10.1029/2005JA011304.

Liu, J., B. Zhao, and L. Liu (2010), Time delay and duration of ionospheric total electron content responses to geomagnetic disturbances, *Ann. Geophys.*, *28*, 795–805, doi:10.5194/angeo-28-795-2010.

Liu, J., L. Liu, B. Zhao, J. Lei, J. P. Thayer, and R. L. McPherron (2012a), Superposed epoch analyses of thermospheric response to CIRs: Solar cycle and seasonal dependencies, *J. Geophys. Res.*, *117*, A00L10, doi:10.1029/2011JA017315.

Liu, J., L. Liu, B. Zhao, Y. Wei, L. Hu, and B. Xiong (2012b), High-speed stream impacts on the equatorial ionization anomaly region during the deep solar minimum year 2008, *J. Geophys. Res.*, *117*, A10304, doi:10.1029/2012JA018015.

Liu, L., W. Wan, B. Ning, H. Yuan, and J. Y. Liu (2002), Low latitude ionospheric effects near 120°E during the great geomagnetic storm of July 2000, *Sci. China (Ser. A)*, *45*(supp l), 148–155.

Lu, G., L. Goncharenko, M. J. Nicolls, A. Maute, A. Coster, and L. J. Paxton (2012), Ionospheric and thermospheric variations associated with prompt penetration electric fields, *J. Geophys. Res.*, *117*, A08312, doi:10.1029/2012JA017769.

Mannucci, A. J., B. T. Tsurutani, B. A. Iijima, A. Komjathy, A. Saito, W. D. Gonzalez, F. L. Guarnieri, J. U. Kozyra, and R. Skoug (2005), Dayside global ionospheric response to the major inter-planetary events of October 29–30, 2003 "Halloween Storms", *Geophys. Res. Lett.*, *32*, L12S02, doi:10.1029/2004GL021467.

Mao, T., W. Wan, X. Yue, L. Sun, B. Zhao, and J. Guo (2008), An empirical orthogonal function model of total electron content over China, *Radio Sci.*, *43*, RS2009, doi:10.1029/2007RS003629.

Maruyama, N., A. D. Richmond, T. J. Fuller-Rowell, M. V. Codrescu, S. Sazykin, F. R. Toffoletto, R. W. Spiro, and G. H. Millward (2005), Interaction between direct penetration and disturbance dynamo electric fields in the storm-time equatorial ionosphere, *Geophys. Res. Lett.*, *32*, L17105, doi:10.1029/2005GL023763.

Mendillo, M. (2006), Storms in the ionosphere: Patterns and processes for total electron content, *Rev. Geophys.*, *44*, RG4001, doi:10.1029/2005RG000193.

Nishida, A. (1968), Coherence of geomagnetic DP 2 fluctuations with interplanetary magnetic variations, *J. Geophys. Res.*, *73*(17), 5549–5559, doi:10.1029/JA073i017p05549.

Prölss, G. W. (1995), Ionospheric F-region storms, in *Handbook of Atmospheric Electrodynamics*, vol. 2, edited by H. Volland, pp. 195–248, CRC press, Boca Ration, Fla.

Prölss, G. W., and M. J. Jung (1978), Traveling atmospheric disturbances as a possible explanation for daytime positive storm effects of moderate duration at middle latitudes, *J. Atmos. Terr. Phys.*, *40*, 1351–1354.

Reinisch, B. W., et al. (2009), New Digisonde for research and monitoring applications, *Radio Sci.*, *44*, RS0A24, doi:10.1029/2008RS004115.

Richmond, A. D., and G. Lu (2000), Upper-atmospheric effects of magnetic storms: A brief tutorial, *J. Atmos. Sol. Terr. Phys.*, *62*, 1115–1127.

Richmond, A. D., C. Peymirat, and R. G. Roble (2003), Long-lasting disturbances in the equatorial ionospheric electric field simulated with a coupled magnetosphere-ionosphere-thermosphere model, *J. Geophys. Res.*, *108*(A3), 1118, doi:10.1029/2002JA009758.

Rishbeth, H., R. A. Heelis, J. J. Makela, and S. Basu (2010), Storming the Bastille: The effect of electric fields on the ionospheric F-layer, *Ann. Geophys.*, *28*, 977–981.

Rodrigues, F. S., G. Crowley, S. M. I. Azeem, and R. A. Heelis (2011), C/NOFS observations of the equatorial ionospheric electric field response to the 2009 major sudden stratospheric warming event, *J. Geophys. Res.*, *116*, A09316, doi:10.1029/2011JA016660.

Rostoker, G. (1996), Phenomenology and physics of magnetospheric substorms, *J. Geophys. Res.*, *97*, 12,955–12,973, doi:10.1029/96JA00127.

Santos, A. M., M. A. Abdu, J. H. A. Sobral, D. Koga, P. A. B. Nogueira, and C. M. N. Candido (2012), Strong longitudinal difference in ionospheric responses over Fortaleza (Brazil) and Jicamarca (Peru) during the January 2005 magnetic storm, dominated by northward IMF, *J. Geophys. Res.*, *117*, A08333, doi:10.1029/2012JA017604.

Scherliess, L., and B. G. Fejer (1997), Storm time dependence of equatorial disturbance dynamo zonal electric fields, *J. Geophys. Res.*, *102*(A11), 24,037–24,046, doi:10.1029/97JA02165.

Seaton, M. J. (1956), A possible explanation of the drop in F-region critical densities accompanying major ionospheric storms, *J. Atmos. Terr. Phys.*, *8*, 122–124.

Sobral, J. H. A., M. A. Abdu, C. S. Yamashita, W. D. Gonzalez, A. Clua de Gonzalez, I. S. Batista, C. J. Zamlutti, and B. T. Tsurutani (2001), Responses of the low-latitude ionosphere to very intense geomagnetic storms, *J. Atmos. Sol. Terr. Phys.*, *63*, 965–974, doi:10.1016/S13646826(00)00197-8.

Sojka, J. J., M. David, R. W. Schunk, and R. A. Heelis (2012), A modeling study of the longitudinal dependence of storm time midlatitude dayside total electron content enhancements, *J. Geophys. Res.*, *117*, A02315, doi:10.1029/2011JA017000.

Spiro, R. W., R. A. Wolf, and B. G. Fejer (1988), Penetration of high-latitude electric-field effects to low latitudes during SUNDIAL 1984, *Ann. Geophys.*, *6*, 39–50.

Stankov, S. M., K. Stegen, and R. Warnant (2010), Seasonal variations of storm-TEC at European middle latitudes, *Adv. Space Res.*, *46*, 1318–1325, doi:10.1016/j.asr.2010.07.017.

Strickland, D. J., R. R. Meier, R. L. Walterscheid, J. D. Craven, A. B. Christensen, L. J. Paxton, D. Morrison, and G. Crowley (2004), Quiet-time seasonal behavior of the thermosphere seen in the far ultraviolet dayglow, *J. Geophys. Res.*, *109*, A01302, doi:10.1029/2003JA010220.

Wang, W., J. Lei, A. G. Burns, S. C. Solomon, M. Wiltberger, J. Xu, Y. Zhang, L. Paxton, and A. Coster (2010), Ionospheric response to the initial phase of geomagnetic storms: Common features, *J. Geophys. Res.*, *115*, A07321, doi:10.1029/2009JA014461.

Wei, Y., et al. (2009), Westward ionospheric electric field perturbations on the dayside associated with substorm processes, *J. Geophys. Res.*, *114*, A12209, doi:10.1029/2009JA014445.

Wei, Y., W. Wan, Z. Pu, M. Hong, Q. Zong, J. Guo, B. Zhao, and Z. Ren (2011), The transition to overshielding after sharp and gradual interplanetary magnetic field northward turning, *J. Geophys. Res.*, *116*, A01211, doi:10.1029/2010JA015985.

Wolf, R. A., R. W. Spiro, S. Sazykin, and F. R. Toffoletto (2007), How the Earth's inner magnetosphere works: An evolving picture, *J. Atmos. Sol. Terr. Phys.*, *69*(3), 288–302, doi:10.1016/j.jastp.2006.07.026.

Zhao, B., W. Wan, and L. Liu (2005), Response of equatorial anomaly to the October–November 2003 superstorm, *Ann. Geophys.*, *23*, 693–706.

Zhao, B., et al. (2008), Ionosphere disturbances observed throughout Southeast Asia of the superstorm of 20–22 November 2003, *J. Geophys. Res.*, *113*, A00A04, doi:10.1029/2008JA013054.